Eddy transport and mixing in a wind and buoyancy driven jet on the sphere

Ivana Cerovečki, R. Alan Plumb and William Heres

Program in Atmospheres, Oceans and Climate

Dept. of Earth, Atmospheric, and Planetary Sciences

Massachusetts Institute of Technology

March 23, 2006

E-mail: ivana@rossby.mit.edu

Abstract

The baroclinically unstable wind- and buoyancy- driven flow in a zonally reentrant pie-shaped sector on a sphere is numerically modeled and analyzed using the transformed Eulerian mean (TEM) approach. The very large latitudinal extent of the basin (-50.7 ^{o} latitude to the equator) allows the latitude variation of the Coriolis parameter to strongly influence the flow. Persistent zonal jets are observed in the statistically steady state. Reynolds stress terms play an important role in redistributing zonal angular momentum: convergence of the lateral momentum flux gives rise to a strong eastward jet, with an adjacent westward jet equatorward, and weaker multiple jets poleward. An equally prominent feature of the flow is a strong and persistent eddy that has the structure of a Kelvin's cat's eye and generally occupies the zonal width of the basin at latitudes -15 ^{o} to -10 ^{o} .

A strongly mixed surface diabatic zone overlies the near-adiabatic interior, within which Ertel potential vorticity (but not thickness) is homogenized along the mean isopycnals everywhere in the basin where eddies have developed, except equatorward of the most energetic eastward jet. A region of low PV is formed adjacent to the strong baroclinic front associated with that jet and subsequently maintained by strong convective events.

The eddy buoyancy flux is dominated by its skew component over large parts of the near-adiabatic interior, with diapycnal components present only in the vicinity of the main jet and in the surface diabatic layer. Close to the main jet, the diapycnal components are dominantly balanced by the triple correlation terms in the buoyancy variance budget, while the advection of buoyancy variance by the mean flow is not a dominant term in the eddy buoyancy budget.

Along-isopycnal mixing in the near-adiabatic interior is estimated by applying the effective diffusivity diagnostic of Nakamura (1996). Diffusivity is large at the flanks of and beneath the main jet and small in the the jet core.

1 Introduction

Large scale ocean circulation models used to study and model the circulation of the ocean must parameterize the effects of unresolved baroclinic eddies that affect the time-mean circulation through the transfer of heat and dynamic tracers, such as potential vorticity (PV). Much progress has been made recently in understanding the role of mesoscale eddies in developing and maintaining the ocean stratification (*e.g.* Karsten et al., 2002; Marshall and Radko, 2003; Radko and Marshall, 2004; Kuo et al., 2005), as well as in developing the theory and parameterization of eddy transport (*e.g.* Gent and McWilliams, 1990; Gent et al., 1995; McDougall and McIntosh, 1996; Treguier et al., 1997; Visbeck et al., 1997; Greatbatch, 1998; Wilson and Williams, 2004; Plumb and Ferrari, 2005).

With the aim of developing further our understanding of eddy transport and its impact on the mean state of the ocean, we here build on two recent studies. Plumb and Ferrari (2005) have developed a nongeostrophic transformed Eulerian-mean (TEM) theory for analysis of eddy transport of zonal mean flow, while Kuo et al. (2005) applied the theory to diagnose the equilibrium state of a wind- and buoyancy-driven, baroclinically unstable re-entrant flow on an f-plane. Like Treguier et al. (1997), Kuo et al. found that the role of eddies in that case could be interpreted in a straightforward way in terms of mixing of PV in the near-adiabatic interior and mixing of buoyancy in a diabatic surface layer.

In the present study, we consider a baroclinically unstable flow on the sphere. The model set-up is briefly described in Section 2; the modeled ocean is a sector of the sphere between the equator and 50.7^o south latitude, and 10^o width (with periodic bondary conditions) in longitude. The flow, forced by an eastward wind stress and thermal relaxation at the surface, becomes baroclinically unstable and eventually reaches a statistically steady state characterized by oceanically realistic flow speeds and stratification; these and other aspects of the mean state are described in Section 3. One important feature of the equilibrated flow

is that over much of the domain the mean Ertel potential vorticity is homogenized along the mean isopycnals. The role of eddies in maintaining the equilibrium state is discussed in Section 4 within the framework of the TEM formalism. The residual circulation and residual fluxes of buoyancy and PV are weak in the near-adiabatic interior except in the vicinity of the main jet. "Eddy drag," which represents eddy forcing in the momentum equation and which can be represented as a function of residual PV flux along the mean isopycnals and the diapycnal buoyancy flux (Plumb and Ferrari, 2005), is weak except near the top and bottom boundaries.

In order to quantify the along-isopycnal, eddy-induced, mixing in the flow, we use the "effective diffusivity"diagnostic developed by Nakamura (1996) and Winters and D'Asaro (1996). This is done by introducing a tracer into the flow, conserved everywhere but in the top model layer, except for a weak diffusivity, and using the resulting tracer structure to determine the spatially dependent effective diffusivity, as described in Section 5. In agreement with chaotic advection theory, with experience in atmospheric applications (Haynes and Shuckburgh, 2000 a, b), and with the recent results of Marshall et al. (2005) for the Antarctic Circumpolar Current, effective diffusivity is found to be large on the flanks of, and beneath, the main zonal jet with lower values in the core of the jet. Our conclusions are summarized in Section 6.

2 Model set-up

The model used is the MITgcm (Marshall at al. 1997 a,b) configured in spherical coordinates. We consider hydrostatic flow in a domain between -50.7 ^{o} and the equator on the sphere. The equation of state is linear: $\rho = \rho_0(1 - \alpha_T T)$, where ρ is density, ρ_0 is reference density, α_T is the thermal expansion coefficient and T is temperature. The boundary conditions on velocity field are no slip at -50.7^o and free slip at the equator. The horizontal resolution

of 1/6 of a degree is eddy-permitting, but in the interests of computational economy we restrict the basin width to 10 degrees of longitude with periodic boundary conditions. The modeled ocean has 15 vertical levels of variable depth between the surface and the flat ocean bottom at 4 km depth, where momentum is removed by quadratic bottom drag with a drag coefficient $C_D = 0.01$ m^2 s^{-1}.

Small scale variance is dissipated by (in the vertical) harmonic and (in the horizontal) biharmonic diffusion of momentum and buoyancy as well as convective adjustment of unstably stratified regions of fluid columns. In the uppermost three layers, of 100 m total thickness, the vertical viscosity and diffusivity are taken to be $A_z = K_z$=10^{-2} m^2 s^{-1}, in order to simulate a mixed layer. Elsewhere, K_z=3x10^{-5} m^2 s^{-1} and A_z=10^{-3} m^2 s^{-1}. The biharmonic diffusion coefficients are K_H=10^{10} m^4 s^{-1} for temperature and A_H=2x$10^{11}$$m^4 s^{-1}$ for momentum.

The flow is forced at the surface by wind stress and buoyancy forcing. The buoyancy forcing is imposed by requiring the upper surface temperature to relax to a specified equilibrium distribution with the relaxation time of 30 days. The applied wind stress and equilibrium temperature are shown in Figure 1. The wind stress is everywhere eastward (there is no westward stress in low latitudes) and becomes very small within about 10 degrees of the equator; it reaches a maximum at 33^{o}S, resulting in Ekman downwelling equatorward of the maximum and Ekman upwelling poleward.

The model was integrated from a state of rest and horizontally uniform stratification with realistic buoyancy frequency. The flow quickly became baroclinically unstable and the imposed forcing, in collusion with baroclinic eddies, resulted in a statistically steady state after several hundred years. All results presented here are taken after this steady state has been attained; the flow was integrated for 1285 years and the results were averaged in time over the last 100 years.

3 The equilibrium state description

3.1 Zonal means

The upper panel of Fig. 2 shows the equilibrium distribution of the zonally and time averaged temperature field. Convective adjustment in the cold southern part of the basin mixes the entire fluid column vertically to nearly uniform density. Between about -10^o and -15^o latitude, the isotherms spread apart at depths of about 200 m to 800 m, forming a well defined pool of large thickness and thus of low PV. Closer to the Equator, both the wind and the surface heating are weak, and the fluid column remains uniformly stratified to great depth.

The lower panel of Figure 2 shows the zonally and time averaged zonal flow. A strong, deep, eastward jet is present just poleward of -15^o with several additional eastward, albeit successively weaker, jets poleward of -26^o. The mean zonal flow reverses direction suddenly on the equatorward side of the main jet, where the flow is westward, peaking near -13 ^{o}.

It is well known that both barotropic and baroclinic flows whose forcing, as in this case, extends over many deformation radii in latitude, develop multiple jets (e.g., Panetta 1993), a result of the important role of Reynold's stresses in redistributing zonal angular momentum and thus determining the structure of the zonal mean flow. The time average of the three terms in the vertically integrated momentum balance,

$$-\frac{\partial}{\partial y}\int_{-D}^{0} \overline{u'v'}\, dz + \frac{1}{\rho}\left(\tau_0 - \tau_{-D}\right) = 0 \ , \tag{1}$$

where τ_0 is the applied wind stress and τ_{-D} the bottom stress, are shown in Figure 3. While the bottom stress mirrors the wind stress in its broad features, it also shows the presence of the jets (which extend down to the bottom, albeit weakly). The difference between top and bottom stress is balanced by the Reynolds stress divergence, as (1) implies. Angular momentum put in by the wind stress at the surface is thus redistributed latitudinally by the eddies and taken up by the bottom drag.

While the zonal mean flow has essentially equilibrated by this time, it is not in fact steady, but fluctuates quasi-periodically. The main eastward jet oscillates laterally about its mean position in a manner similar to what is found in simple models of the atmosphere, where fluctuations of the jet take the form of "annular modes" (e.g. Kushner and Polvani, 2004) and which in turn appear to be analogs of similar behavior in the real atmosphere (e.g., Thomson and Wallace, 2000). In our case, with multiple jets, the behavior is more complex: during each period, the secondary jets in fact migrate systematically equatorward, the northernmost one merging with the main jet while a new jet appears to the south. This behavior, a consequence of the mutual interaction between eddies and the jets, is explored further in Chan et al. (2006).

3.2 Eddy structures

Figure 4 shows a snap-shot of sea surface temperature as a function of latitude and longitude (note that three zonal periods are plotted in the figure). Eddy activity is mostly confined between -10^o and -35 ^{o} latitude. The dominant and strongly persistent feature is a single cold eddy (i.e., zonal wavenumber one within the 10^o longitude domain) found just equatorward of the main eastward jet. It is likely that the size of this eddy is determined by the geometry of the basin — at the beginning of the calculation it grew in size until it become zonally as large as the geometry permits. Poleward of the main jet, eddies of smaller scale are evident.

The circulation around the dominant cold eddy is anticyclonic. The temperature structure equatorward of the jet is very similar to that of a classic critical layer (Haynes,1985), the cold eddy taking the form of a Kelvin's cat's eye — a lens shaped region of closed streamlines enclosing a well mixed region. In this critical layer between the eastward and westward jets where the mean flow is weak (the zonal phase speed of this eddy $c \simeq 0.1\mathrm{ms}^{-1}$eastward, and the critical layer forms where $\bar{u} \simeq c$), the flow is essentially trapped within the eddy. As Figure 4 shows, both warm and cold water filaments are formed at the apex of the eddy

(similar to the hyperbolic point in a steady flow). At the time of Figure 4, the eddy is very close to the jet, but it subsequently drifts slowly equatorward, weakens and is advected eastward by the local flow. Subsequently, it reforms near the jet and the cycle repeats itself.

As the warm water filaments are wrapped around the eddy on its poleward side, they fill a growing region between the eddy and the eastward jet with warm water. This region therefore becomes prone to convection since the atmosphere above is colder than the surface water. Convective events and the subsequent sliding of water along isopycnals carry surface water downward into the interior, feeding the low PV pool that is visible as the weakly stratified region between latitudes of -10 ^{o} to -15 ^{o}, and depths of 200 m to 800 m, in Fig. 2. This process is discussed further by Cerovečki and Marshall (*submitted*).

3.3 Eddy heat fluxes

The zonal- and time-mean eddy heat flux $\overline{\mathbf{v}'T'}$ is shown in Figure 5 superposed on zonally averaged isotherms (which coincide with the isopycnals in this calculation). The eddy heat flux has a large, downgradient diapycnal component in the surface diabatic layer; however it is "skew" (along the mean isopycnals) almost everywhere in the adiabatic interior, the exception being at the equatorward edge of the main jet, at about -15^{o}S, where the flux is diapycnal and mostly upgradient. The presence of this apparently diapycnal region is at first sight surprising, since the diabatic terms are everywhere small in the interior; as is well known, the diabatic component of the eddy buoyancy flux can be related to a diabatic term and the advection of buoyancy variance:

$$\overline{\mathbf{u}'b'} \cdot \nabla \bar{b} = \overline{b'Q'} - \left(\frac{\partial}{\partial t} + \bar{\mathbf{u}} \cdot \nabla \right) \left(\frac{1}{2} \overline{b'^2} \right) - \nabla \cdot \left(\frac{1}{2} \overline{\mathbf{u}' b'^2} \right) \tag{2}$$

where Q' is the diabatic source (or sink) of buoyancy. If mean and eddy advection of the eddy buoyancy variance is negligible, there is in a statistically steady state a direct relationship between diapycnal eddy fluxes and local diabatic processes. However, analysis of this budget

shows that in the region equatorward of the main jet the diapycnal fluxes are not in fact indicative of local diabatic processes, but of the advection of buoyancy variance; in fact, it is here eddy advection (i.e., the triple correlation term) that dominates the right hand side of (2). Wilson and Williams (2004) pointed to the potential importance of the triple correlation terms in the PV budget.

3.4 Distribution of mean PV and thickness

Figure 7 shows the distribution of the zonally and time averaged Ertel potential vorticity superposed on mean isopycnals (isotherms). Figure 6 shows the zonal and time averaged thickness superposed on mean density (temperature) surfaces. Comparison of this figure with Figure 7 shows that, in the region of active eddies near and poleward of the main jet, it is PV rather than thickness that is homogenized along isopycnals.

It is clear in Figure 7 that in and poleward of the main jet, PV is homogenized[1] along the mean isopycnals in the near-adiabatic interior, but not near the surface. However, equatorward of about -12^o, where eddies are weak, strong along-isopycnal gradients of mean PV persist at the edge of the homogenized region. Within the region of along-isopycnal homogenization, the mean PV field varies non monotonically with buoyancy. A tongue of strongly cyclonic PV extends downward and equatorward from the surface at about -23^o to a depth of about 1500 m at $-15\ ^o$. Above the equatorward termination of this tongue lies the low PV pool noted above.

[1]We note that the PV shown in Figure 7 is the unweighted mean PV, i.e. $\bar{P} = \overline{\zeta_a \cdot \nabla T}$ rather than the thickness weighted mean, $\bar{P}^* = \bar{\zeta}_{\mathbf{a}} \cdot \nabla \bar{\mathbf{T}}$. The latter is not as well homogenized within the jet as is the quantity shown in the figure.

4 Transformed Eulerian Mean (TEM) analysis

4.1 Residual circulation

The TEM equations rely on the transformation from the Eulerian mean velocity $\bar{\mathbf{u}}$ to the residual mean velocity $\bar{\mathbf{u}}^{\dagger}$, where

$$\bar{\mathbf{u}}^{\dagger} = \bar{\mathbf{u}} + \nabla \times \mathbf{i}\psi, \tag{3}$$

where $\mathbf{i}$ is the unit vector in the x-direction and ψ is the "quasi-Stokes " streamfunction. Andrews and McIntyre (1978) introduced the coordinate-independent form of the quasi-Stokes streamfunction

$$\psi = -\frac{\mathbf{s} \cdot \overline{\mathbf{u}'\mathbf{b}'}}{\left|\nabla \bar{b}\right|} = \frac{-\overline{v'b'}\bar{b}_z + \overline{w'b'}\bar{b}_y}{\bar{b}_y^2 + \bar{b}_z^2}, \tag{4}$$

in which $\mathbf{s}$ is a unit vector parallel to the zonal mean isopycnal surface given by $\mathbf{s} = \mathbf{n} \times \mathbf{i}$ (where $\mathbf{n}$ is a unit vector normal to the zonal mean isopycnal surface, so that $\mathbf{s}$ is northward, along the mean isopycnals, for stable stratification). Plumb and Ferrari (2005) argued that it is advantageous to use the definition (4) of the quasi-Stokes streamfunction, in which the buoyancy flux and gradient are referenced to the local mean isopycnal slope, thus providing in general the cleanest separation of the diapycnal and isopycnal flux components. They further showed when using this definition of the quasi-Stokes streamfunction, the surface boundary condition can be dealt with more readily than when using QG definition of the quasi-Stokes streamfunction, because in the presence of a mixed layer where $\partial b/\partial z = 0$, isopycnals become locally vertical and (4) automatically satisfies a condition $\psi = 0$ at the upper boundary (in fact equaling the expression of Held and Schneider (1999) within the mixed layer). However, PF noted that while this condition (which really requires $|\partial b/\partial z| \ll |\partial b/\partial y|$) may be satisifed in laboratory systems like that analyzed by Kuo et al. (2005), it is unlikely to be met in systems with realistic aspect ratio (such as the case of interest here), where $|\partial b/\partial z| \gg |\partial b/\partial y|$ even in the mixed layer.

One way around this difficulty is to stretch coordinates in the vertical by a factor γ, the inverse of a representative aspect ratio, to make the aspect ratio of order unity in the stretched coordinates, in which case (4) becomes

$$\psi = \frac{-\overline{v'b'}\bar{b}_z + \gamma^2\overline{w'b'}\bar{b}_y}{\gamma^2\bar{b}_y^2 + \bar{b}_z^2} \ . \tag{5}$$

Alternatively, we can exploit the inherent nonuniqueness in ψ. Plumb and Ferrari (2005) introduced a more general definition of the quasi-Stokes streamfunction:

$$\psi \equiv -\left|\nabla\bar{b}\right|^{-1}\left[\mathbf{s}\cdot\overline{\mathbf{u}'\mathbf{b}'} - \alpha\left(\mathbf{n}\cdot\overline{\mathbf{u}'\mathbf{b}'}\right)\right]. \tag{6}$$

In fact, it is straightforward to show that (5) and (6) are equivalent if

$$\alpha = \frac{\epsilon(1-\gamma^2)}{1+\epsilon^2\gamma^2} \tag{7}$$

where $\epsilon = -\bar{b}_y/\bar{b}_z$ is the mean isopycnal slope. Accordingly, we chose $\gamma = \gamma_0\varepsilon$, where a value $\gamma_0 = 10^3$, a value that makes the interior isopycnal slopes of order unity in the streched coordinate, and which makes the upper boundary condition on ψ very close to zero.

Figure 8 shows that the quasi-Stokes streamfunction as defined by (5) does indeed produce a closed circulation. This streamfunction also agrees well with that of Held and Schneider (1999) close to the surface, and with the conventional (quasi-geostrophic) definition in the near-adiabatic interior, except that our form remains well-defined and smooth in the far south part of the basin where the stratification is very weak whereas the latter takes on unrealistically large values. As shown in Figure 9, the residual circulation thus defined is smooth, merges smoothly with the boundary conditions, and has about 10 per cent of the Eulerian mean transport in the interior . To a first approximation, the residual circulation is confined to the mixed layer.

4.2 Angular momentum flux

Figure 10 shows the residual eddy angular momentum flux $\mathbf{F}^\dagger\{m\}$, where $m = 2\Omega a^2 \cos^2\phi + ua\cos\phi$ is the specific angular momentum, and

$$\mathbf{F}^\dagger\{\mathbf{m}\} = \overline{\mathbf{u'm'}} - \psi \mathbf{i} \times \nabla \bar{\mathbf{m}} \ . \tag{8}$$

The divergence of this flux represents the eddy forcing term in the TEM momentum equation

$$\frac{\partial \bar{m}}{\partial t} + \bar{\mathbf{u}}^\dagger \cdot \nabla \bar{\mathbf{m}} = -\nabla \cdot \mathbf{F}^\dagger\{\mathbf{m}\} + \mathbf{a}\cos\phi \, \frac{\partial \tau}{\partial \mathbf{z}} \ . \tag{9}$$

The surface wind stress input of zonal angular momentum is shown in Figure 1 with a maximum around $-33\ ^o$. As, *e.g.*, in the f-plane case of Kuo et al. (2005), in the TEM budget it is vertical momentum transport by the eddies, and not by the mean circulation, that transfers the wind stress downward to be removed by the bottom stress. In contrast to Kuo et al. (2005), however, there is also significant horizontal momentum transport by the Reynolds' stresses evident as the latitudinal component of $\mathbf{F}^\dagger\{m\}$, especially in the upper 500m; zonal momentum is thus transferred predominantly into the core of the main jet. Except close to the upper and lower boundaries, the flux is almost nondivergent, consistent with a very weak residual flow in the equilibrium state.

Plumb and Ferrari (2005) showed that for small Rossby number, but arbitrary isopycnal slope, there is a simple relationship between the TEM momentum flux divergence and the eddy PV and buoyancy fluxes. They used $\alpha = 0$ in the definition of ψ in (6); with our choice of nonzero α, the relationship becomes

$$\nabla\cdot\mathbf{F}^\dagger\{m\} = -\left|\nabla\bar{b}\right|^{-1} \left\{ F^{\dagger(s)}\{P\} - \left[f\frac{\bar{b}_z^2}{\left|\nabla\bar{b}\right|^2}\left(\frac{\bar{b}_y}{\bar{b}_z}\right)_z - \frac{df}{dy}\frac{\bar{b}_y^2}{\left|\nabla\bar{b}\right|^2}\right] F^{\dagger(n)}\{b\} \right\} + f\frac{\partial}{\partial z}\left(\frac{\alpha}{\left|\nabla\bar{b}\right|} F^{\dagger(n)}\{b\} \right) \ . \tag{10}$$

In Eq. (10) eddy forcing of the mean angular momentum has been expressed in terms of the fluxes of two materially conserved quantities – the diapycnal flux of buoyancy and the isopycnal flux of PV.

Figure 11 shows eddy forcing of the mean angular momentum, given by $-\nabla \cdot \mathbf{F}^{\dagger}\{m\}$. The flux is almost nondivergent in the interior, except in the region of the main jet, above 1000 m depth and between about 13^o and 20^oS, where as already noted, the buoyancy fluxes have a significant diapycnal component because of eddy advection of buoyancy variance. The flux is strongly divergent in the mixed layer, and convergent near the bottom boundary, consistent with eddy angular momentum transfer from the surface down to the bottom, as discussed above. In terms of the four terms on the right side of (10), the second and third are negligible everywhere, consistent with scaling analysis, which shows them to be significant only where the isopycnal slopes are of order unity (Plumb and Ferrari, 2005). The first term, the isopycnal residual PV flux, provides the angular momentum flux convergence at the bottom, while both the first and last terms contribute to the net divergence in the near-jet interior region. The same two terms also contribute to the angular momentum flux divergence in the mixed layer; in fact, these terms largely cancel there, such that $\nabla \cdot \mathbf{F}^{\dagger}\{m\}$ is in fact a small residual of the two. Thus, for example, the Eliassen-Palm flux, $-\mathbf{F}^{\dagger}\{m\}$, that is launched out of the surface layer is smaller than what is implied by the near-surface heat fluxes alone. The importance of the near-boundary PV fluxes is consistent with the arguments of Schneider (2005), though here, at an upper boundary, the PV and heat flux contributions oppose each other, unlike in Schneider's analysis of the lower boundary of an atmospheric model.

Finally, we note the consistency between the pattern of $\nabla \cdot \mathbf{F}^{\dagger}\{m\}$ of Fig. 11 and the residual circulation shown in Fig. 9, as is anticipated by the mean angular momentum budget (9). The near-zero residual flow in the interior, a consequence of weak diabatic effects there, implies the vanishing of $\nabla \cdot \mathbf{F}^{\dagger}\{m\}$ there. Within the mixed layer, there is a recirculating residual flow, driven equatorward by the surface wind stress and poleward below, by the eddy flux divergence; the similar circulation near the bottom exists for the same reasons.

5 Effective diffusivity as a diagnostic of mixing

5.1 Theoretical background

"Effective diffusivity" was introduced by Nakamura (1996) and Winters and D'Asaro (1996) who showed that the combined effects of advection and diffusion, when described by the two-dimensional advection-diffusion equation

$$c_t + \mathbf{u} \cdot \nabla c = \nabla \cdot (\kappa \nabla c), \tag{11}$$

where $c(\mathbf{x}, t)$ is tracer concentration, κ is a constant diffusivity and $\mathbf{u}(\mathbf{x}, t)$ is a two-dimensional non-divergent velocity field, can be described exactly as a diffusion in tracer-based coordinates. Taking a "modified Lagrangian mean" approach, in which averages are taken along contours of the almost-conserved tracer, leads to the equation

$$\frac{\partial C}{\partial t} = \frac{1}{a^2 cos\phi_e} \frac{\partial}{\partial \phi_e} \left[K_{eff} cos\phi_e \frac{\partial C}{\partial \phi_e} \right], \tag{12}$$

where the "equivalent latitude" $\phi_e(C, t)$ of the contour of tracer concentration C, is defined in terms of the area $A(C, t)$ enclosed by (poleward of) the contour such that $A = 2\pi a^2(1 - sin\phi_e)$, where a is the Earth radius. (If the contour were an undisturbed latitude circle, ϕ_e would just equal the latitude of the contour.) The "effective diffusivity" K_{eff} is

$$K_{eff} = \kappa \frac{L_e^2}{4\pi^2 a^2 cos^2 \phi_e} = \kappa \frac{L_e^2}{L^2(\phi_e)}, \tag{13}$$

where $L(\phi_e) = 2\pi a \cos \phi_e$ is the length of the circle of latitude ϕ_e, and

$$L_e(C) = \sqrt{\oint |\nabla c| dl \ \oint \frac{dl}{|\nabla c|}}, \tag{14}$$

is known as "equivalent length "of the contour (the integrals being around the contour).

From (14) one can see that effective diffusivity is a measure of the geometric complexity of a tracer field. Regions with weak mixing have small stretching rates so the resulting

geometric structure of the tracer field is simple, $L_e \sim L$, and the effective diffusivity is small. On the other hand, effective diffusivity is large if the geometric structure of the tracer field is complex, which is in turn the result of large stretching rates typical for regions with strong mixing. Haynes and Shuckburgh (2000a,b) and Allen and Nakamura (2001) have applied this method to diagnose transport and mixing properties in the stratosphere and troposphere. Marshall et al. (2005) used the same method to estimate surface diffusivities associated with geostrophic eddies in the southern ocean by numerically monitoring lengthening of idealized tracer contours which were being strained by surface geostrophic flow observed by satellite altimetry. Here, we use this method to diagnose mixing properties of the flow with the goal of understanding tracer dynamics for application to a parameterized model.

5.2 Application to idealized tracer field

The model was run with a tracer whose concentration in the uppermost model layer only was relaxed with relaxation time 1 month to a specified latitudinal profile, with concentration increasing linearly with latitude from 0 at 50.67 degrees south to 1 at the equator; a Laplacian horizontal tracer diffusivity $\kappa = 30$ m^2/s was included. Coefficients of eddy diffusivity were diagnosed using (13) and (14) from the modeled tracer field. After an initial adjustment period: we analyzed 40 snapshots of tracer concentration taken at regular time intervals of one year starting 30 years after tracer release, each analysis was carried out on 67 temperature levels defined by the values of the zonally and time averaged SST at points which are 0.67^o latitude apart.

Since we expect the processes of stirring and mixing to occur within isopycnal surfaces under the near-adiabatic conditions that characterize the flow interior (i.e. away from the surface diabatic layer), we analyze tracer distributions on isothermal (isopycnal) surfaces. A balance between advection and diffusion occurs on the scale$\sqrt{\kappa/S}$, where S is the strain rate which can be approximated by the ratio of V/L, where V and L are typical scales for eddy

speed and size. The dominant eddy is as large as geometry permits, so L is approximately 10^o longitude, and a typical velocity scale is 0.1 - 0.2 m/s, which gives a dissipative length scale of approximately 15 km, very close to the model grid scale.

5.3 Results and Discussion

Figure 12 shows instantaneous effective diffusivity estimates (top panel) obtained by analyzing a snapshot of tracer concentration on an isopycnal surface (T=1.3^{o}C, bottom panel). The mixing regions are characterized by tracer concentration contours which are vigorously stretched into complex geometrical shapes with tight gradients: one highly stirred region is between 15^o to 20^o latitude where the tracer concentration contours are stretched to enclose large areas and another is poleward of 25^o latitude. Poleward of about 33^o, effective diffusivity estimates could not be obtained on this isothermal surface, because the surface outcrops and the tracer contours are no longer closed. Equatorward of 12^o latitude and in the region around 23^o-24^o latitude the smoothness of the tracer contours is reflected in small values of effective diffusivity.

Figure 13 shows time-averaged effective diffusivity estimates vs. depth and the equivalent latitude. Contours of the zonal mean zonal velocity are overlaid to illustrate the underlying flow structure. Light lines show the isopycnal surfaces on which effective diffusivity calculation has been carried out and the thick light line is the isothermal surface analyzed in the previous figure.

Figure 13 shows strong spatial inhomogeneity in the distribution of effective diffusivity, which is large on the equatorward side of the strong eastward jet, beneath the jet and on the poleward side of the jet. Centered on the core of the jet is a band of very low effective diffusivity. In the jet core region, the jet simply meanders in time, thus not giving rise to much mixing. Surface temperature contours, shown in Figure 4, illustrate this behavior: in the region of the strong eastward jet (13^o to 19^o latitude) temperature contours are very smooth,

whereas on the equatorward side of the jet temperature contours are vigorously streched, folded and wrapped around the large eddy giving rise to strong temperature gradients and strong mixing. Therefore the region of high effective diffusivity does not coincide with the region of strongest eddy activity, which was shown to coincide with the region occupied by the strong eastward jet (Figure 5), but reflects where chaotic stirring is most vigorous, in the wings of the jet (cf. Figure 4). Indeed, as shown in Figure 13, the band of large K_eff coincides approximately with the 0.1 m/s velocity contour.

This spatial pattern of effective diffusivity is consistent with the theory of Rossby wave critical layers (Haynes, 1985) which shows that particle displacements are large near the critical line, where the Doppler-shifted phase speed is small. This pattern of weak eddy diffusivities inside the jet and strong diffusivities outside the jet is also consistent with analysis of observed geophysical flows: Haynes and Shuckburgh (2000a) diagnosed transport and mixing properties of the isentropic flow in the lower and middle stratosphere using observed winds to advect tracer on isentropic surfaces. They showed that the stratospheric polar jet is characterized by low diffusivities, thus representing a strong barrier to mixing near the core of the jet, and large diffusivities in the weaker mean flow equatorward of the jet. Similarly, Marshall et al. (2005) estimated near surface eddy diffusivities associated with geostrophic eddies in the southern ocean by numerically monitoring the lengthening of idealized tracer contours which was advected by surface geostrophic flow observed by satelite altimetry. They obtained large diffusivities (2000 m^2/s) on the equatorward flank of Antarctic Circumpolar Current and small diffusivities (500 m^2/s) at the jet axis.

Note that the eddy diffusivities are generaly large in the region poleward of -15^o latitude, which is the region where the strong eddies have homogenized PV on the isopycnal surfaces (Figure 7).

The contrast, evident in Figure 13, between weak mixing at the core of the surface jet, and strong mixing beneath the jet, is consistent with observations of the Gulf Stream. Bauer

et al. (1985) showed that in the upper thermocline the transition of water properties inside and outside of the Gulf Stream jet region is sharp, suggesting that water mass exchanges across the Gulf Stream - Slope Water front are limited at these levels. Below this region deep property fields are being efficiently homogenized by mesoscale exchanges across the Gulf-Stream.

6 Conclusions

Although the modeled flow described here is not a very realistic representation of oceanic flow, it develops a number of dynamical features that can be used to illustrate the characteristics of eddy transport in the ocean. Moreover, the stratification and flow speeds are realistic. The flow develops a number of persistent zonal jets in statistically steady state, with the Reynolds' stresses playing an important role in redistributing zonal angular momentum both horizontally and vertically. An equally prominent feature of the flow is a strong and persistent eddy which has Kelvin's cat's eye structure. The eddy is very large in size, typically occupying the zonal width of the basin, situated on the equatorward side of the main eastward jet at latitudes -15^o to -10^o. Smaller eddies develop further poleward.

Running the experiment in spherical geometry over a large latitude band showed clearly that eddy processes homogenize PV and not thickness along the mean buoyancy contours in the near-adiabatic interior everywhere in the basin where eddies have developed, near and poleward of the most energetic eastward jet.

In the vicinity of the main jet, triple correlation terms in the buoyancy variance budget are large and give rise to a significant diabatic component of eddy buoyancy flux. The mean advection of buoyancy variance is not a dominant term in this balance. This situation is in contrast to the frequent neglect of triple correlation terms in the literature. Redefining the streamfunction to include not only the mean advection of buoyancy variance parallel to the

isopycnals (as suggested by Marshall and Shutts (1981), McDougall and McIntosh (1996, 2001)) but also triple correlation terms (as suggested by Greatbach, 2001) did not uniformly reduce the diapycnal component of eddy buoyancy flux in this flow because buoyancy variance advection has a significant diabatic component.

We have diagnozed eddy mixing and trasnport properties of the flow by applying the effective diffusivity diagnostics introduced by Nakamura (1996) and Winters and D' Asaro (1996). Eddy mixing rates are spatially very inhomogeneous: they are large on the equatorward side of the strong eastward jet, beneath the jet and on the poleward side of the jet. In the core of the jet eddy mixing rates are very low . Thus the region of high effective diffusivity does not coincide with the region of the strongest eddy activity centered at the strong eastward jet.

At the jet, eddy behavior is predominantly wavelike, so although the eddy fluxes are very large there, there is little stirring. parallel to the mean buoyancy contours and thus advective in nature. In the wings of the jet, however, stirring is vigorous, characterized by large particle displacements. This spatial pattern of effective diffusivity is consistent with critical layer theory and with analysis of atmospheric and oceanic flows.

Acknowledgements IC would like to thank Jean-Michel Campine whose generous help with numerous numerical issues was most precious. We acknowledge support from NSF, under grant OCE-0426307.

References

Allen, D. R., and N. Nakamura, 2001: A seasonal climatology of effective diffusivity in the stratosphere. *J. Geophys. Res.*, **106**,7917-7935.

Bower, A.S., H.T. Rossby and J.L. Lillibridge 1985: The Gulf Stream Barrier or Blender? *J. Phys. Oceanogr*, **15**, 24–32.

Cerovečki I. and J.C. Marshall: Eddy modulation of air-sea interaction and convection. *submitted to J. Phys. Oceanogr.*

Chan C. J., I. Cerovečki and R. A. Plumb 2006: Eddy-Mean Flow Interaction in a Multiple Zonal Jet Regime. *J. Atmos. Sci., submitted.*

Gent, P. R., and J. C. McWilliams, 1990: Isopycnal mixing in ocean circulation models. *J. Phys. Oceanogr*, **20**, 150–160.

Gent, P. R., J. Willebrand, T. J. McDougall, McWilliams, J. C. 1995: Parameterizing eddy-induced tracer transports in ocean circulation models. *J. Phys. Oceanogr*, **25**, 463–474.

Greatbatch, R. J. 1998: Exploring the relationship between eddy-induced transport velocity, vertical momentum transfer, and the isopycnal flux of potential vorticity. *J. Phys. Oceanogr*, **28**, 422–432.

Haynes, P.H. 1985: Nonlinear instability of a Rossby-wave critical layer. *J. Fluid Mech.*, **161**, 493–511.

Haynes, P.H.,E. Shuckburgh 2000: Effective diffusivity as a diagnostic of atmospheric transport. Part I: Stratosphere. *J. Geophys. Res.*, **105**, 22777–22794.

Haynes, P.H.,E. Shuckburgh 2000: Effective diffusivity as a diagnostic of atmospheric transport. Part II: troposphere and lower stratosphere. *J. Geophys. Res.*, **105**, 22795–22810.

Karsten, R., H. Jones, and J. Marshall, 2002: The role of eddy transfer in setting the stratification and transport of a circumpolar current. *J. Phys. Oceanogr.*, **32**, 39–54.

Kuo, A., R. A. Plumb, and J. Marshall, 2005: Transformed Eulerian mean theory. II:

Potential vorticity homogenization, and the equilibrium of a wind- and buoyancy-driven zonal flow. *J. Phys. Oceanogr.*, **35**, 175–187.

Kushner, P.J.and L.M. Polvani, 2004: Stratosphere-troposphere coupling in a relatively simple AGCM: The role of eddies. *J. Clim.*, **17**, 629–639.

Marshall, J., C. Hill, L. Perelman, and A. Adcroft, 1997: Hydrostatic, quasi-hydrostatic, and nonhydrostatic ocean modeling, *J. Geophysical Res.*, **102(C3)**, 5733-5752.

Marshall, J., A. Adcroft, C. Hill, L. Perelman, and C. Heisey, 1997: A finite-volume, incompressible Navier Stokes model for studies of the ocean on parallel computers, *J. Geophysical Res.*, **102(C3)**, 5753–5766.

Marshall, J.C. and G.J. Shutts 1981: A note on rotational and divergent eddy fluxes, *J. Phys. Oceanog.*, **11**, 1677–1680.

Marshall, J., and T. Radko, 2003: Residual-mean solutions for the Antarctic Circumpolar Current and its associated overturning circulation. *J. Phys. Oceanogr.*, **33**, 2341–2354.

Marshall, J., Shuckburgh, E., Jones, H., Hill, C. 2005: Estimates and implications of surface eddy diffusivity in the southern ocean derived from tracer transport. *J. Phys. Oceanogr., accepted*

McDougall, T. J., and P. C. McIntosh, 1996: The temporal-residual-mean velocity. Part I: Derivation and the scalar conservation equations. *J. Phys. Oceanogr.*, **26**, 2653–2665.

McDougall, T. J., and P. C. McIntosh, 2001: The temporal-residual-mean velocity. Part II: Isopycnal interpretation and the tracer and momentum equations. *J. Phys. Oceanogr.*, **31**, 1222–1246.

Nakamura, N. 1996: Two-dimensional mixing, edge formation, and permeability diagnosed in an area coordinate. *J. Atmos. Sci.*, **53**, 1524–1537.

Panetta, R. L., 1993: Zonal jets in wide baroclinically unstable regions: persistence and scale selection. *J. Atmos. Sci.*, **50**, 2073–2106.

Plumb, R.A., and R. Ferrari, 2005: Transformed Eulerian-Mean Theory. Part I: Nonquasi-

geostrophic Theory for Eddies on a Zonal-Mean Flow. *J. Phys. Oceanogr.*,**35**, 165–174.

Radko, T. and J. Marshall 2004: Eddy-induced diapycnal fluxes and their role in the maintenance of the thermocline. *J. Phys. Oceanogr.*, **34**, 372–383.

Schneider T., 2005:Zonal Momentum Balance, Potential Vorticity Dynamics, and Mass Fluxes on Near-Surface Isentropes. *J. Atmos. Sci.*, **62**, 1884–1900.

Thompson, D. W. J., and J. M. Wallace, 2000: Annular modes in the extratropical circulation. Part I: Month-to-month variability. *J. Clim.*, **13**, 1000–1016.

Treguier, A. M., I. M. Held, and V. D. Larichev, 1997: On the parameterization of the quasigeostrophic eddies in primitive ocean models. *J. Phys. Oceanogr.*, **27**, 567–580.

Visbeck, M., J. Marshall, T. Haine, and M. Spall, 1997: Specification of eddy transfer coefficients in coarse-resolution ocean circulation models.*J. Phys. Oceanogr.*, **27**, 381–402.

Wilson, C., R. G. Williams, 2004: Why are eddy fluxes of potential vorticity difficult to parameterize?. *J. Phys. Oceanogr.*, **34**, 142–155.

Winters K.B., and A. D'Asaro, 1996: Diascalar flux and the rate of *J. Fluid Mech.*, **317**, 179–193.

7 Figures

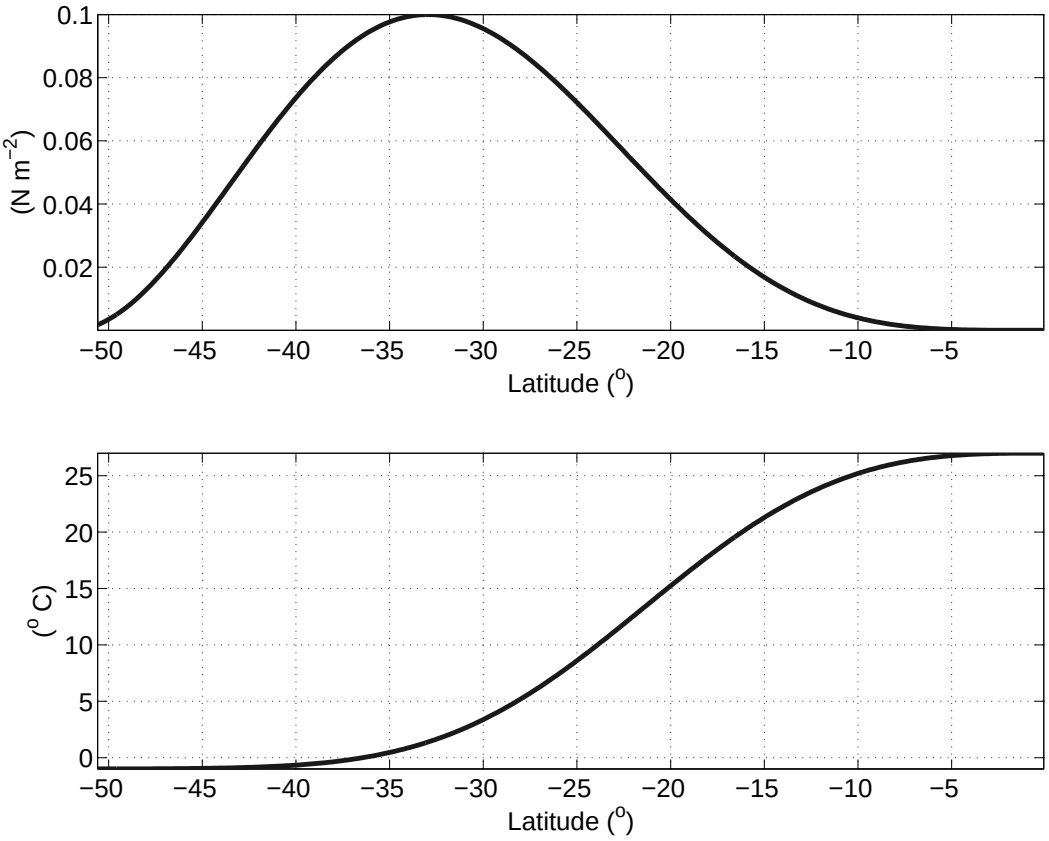

Figure 1: The wind stress forcing τ_S in N/m^2 and the restoring temperature in ^{o}C.

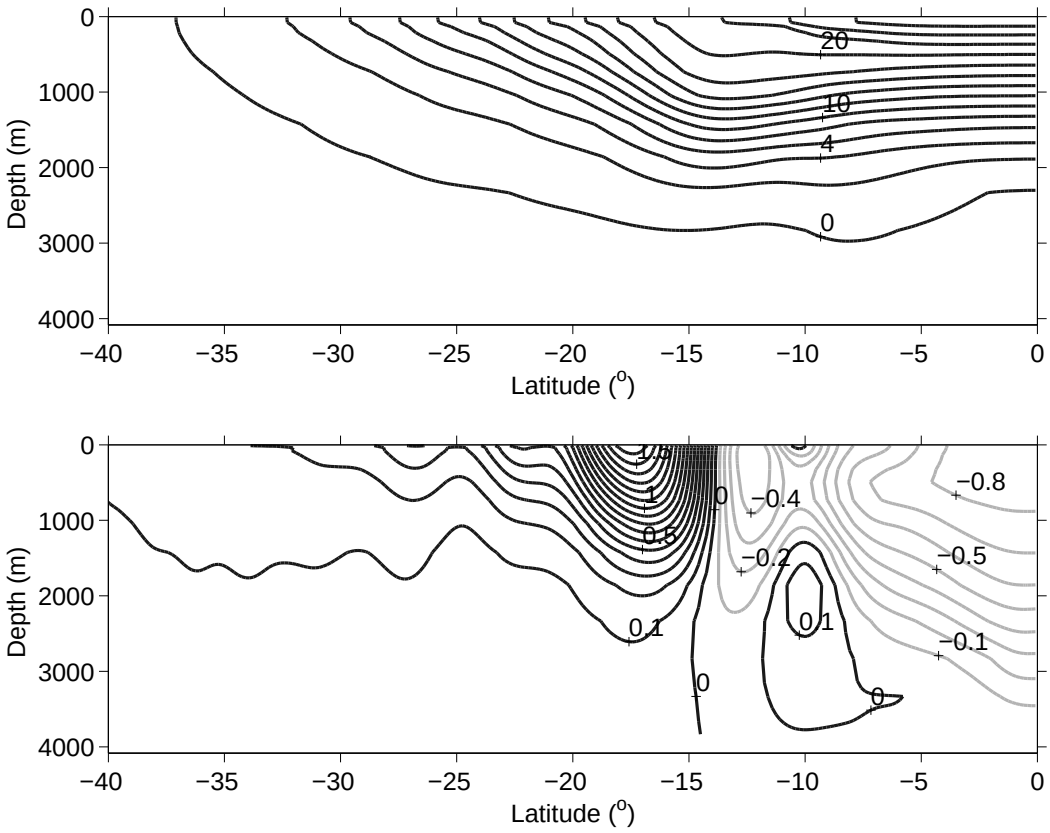

Figure 2: Meridional cross-section of zonally and time averaged: temperature (top panel, in ^{o} C, contour interval is 1 ^{o} C) and zonal velocity (bottom panel, in m s^{-1}), contour interval is 0.1 m s^{-1}). Negative velocities are plotted as a light line. Time averages were taken over 100 years (years 1284-1384 of the run).

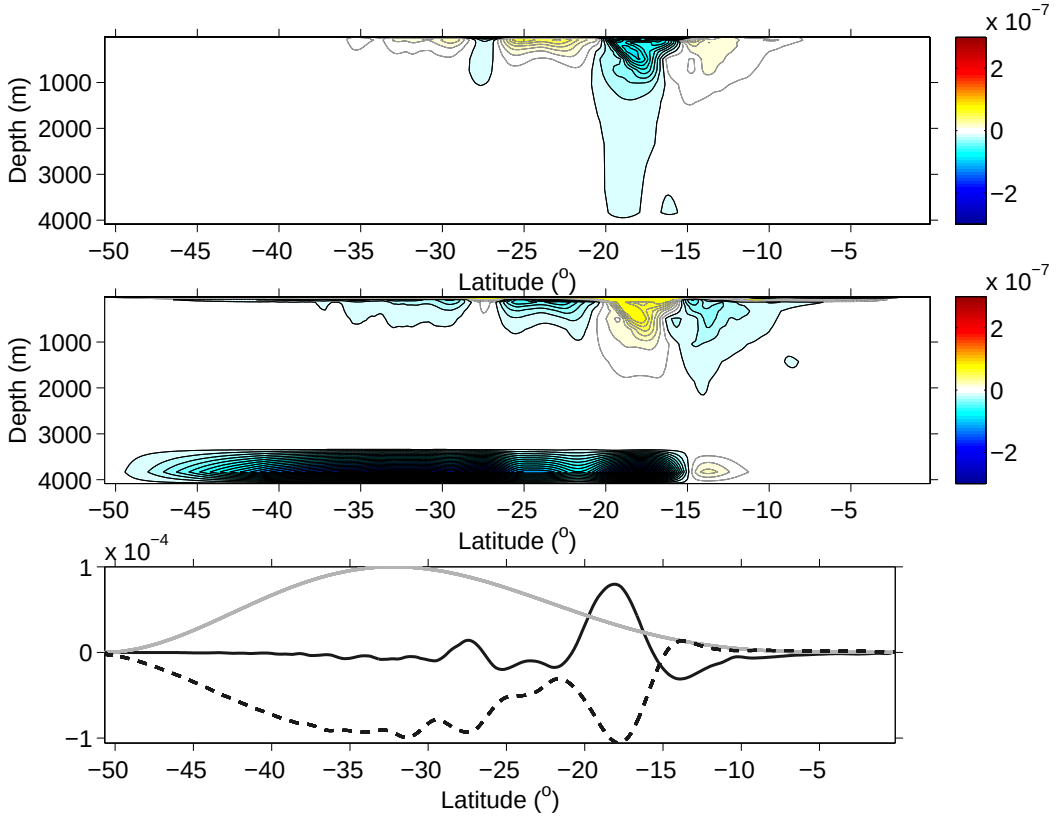

Figure 3: Zonally averaged vertical sections of Reynolds stress divergence $\partial(\overline{u'v'})/\partial y + \partial(\overline{u'w'})/\partial z$ (top panel) and Coriolis acceleration $f\bar{v}$ (middle panel), which are terms that dominate balance in the zonal momentm equation. Contour interval is 10^{-8} m/s^2, positive contours are shown as a light line and negative contours are shown as a dark line. Bottom panel: zonally and time averaged vertically integrated zonal momentum balance: the surface wind stress (light solid line), the vertically integrated Reynolds stress divergence $\partial(\overline{u'v'})/\partial y$ (dark solid line); bottom drag (dashed line). (The vertically integrated Coriolis term must vanish by mass conservation.)

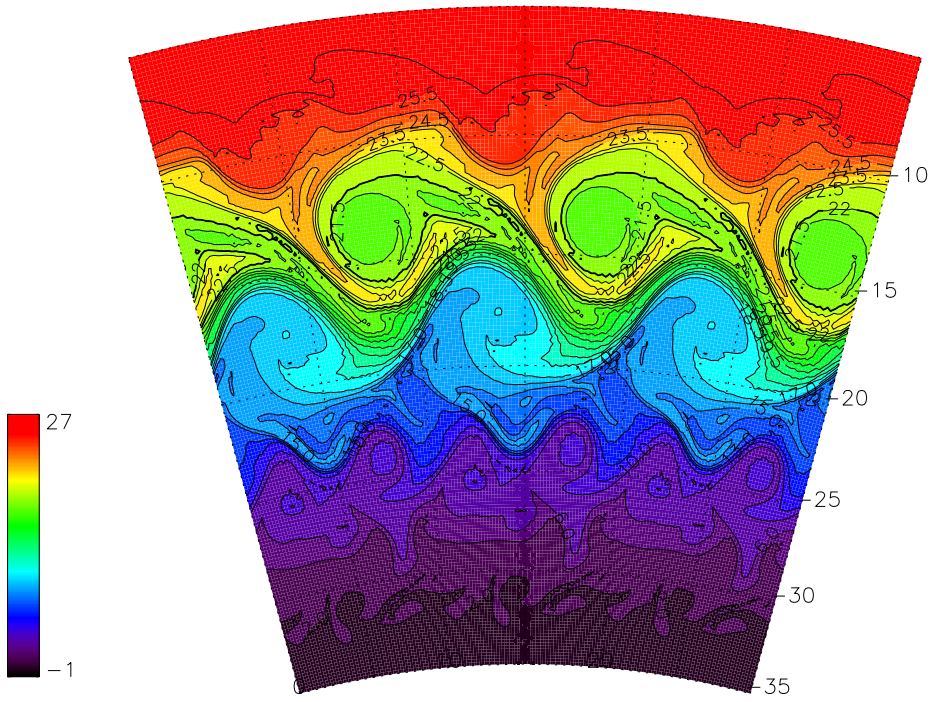

Figure 4: A snap shot of sea surface temperature (^{o}C); the periodic field is plotted three times in longitude, and only latitudes between -5 ^{o} and -35 ^{o} are shown).

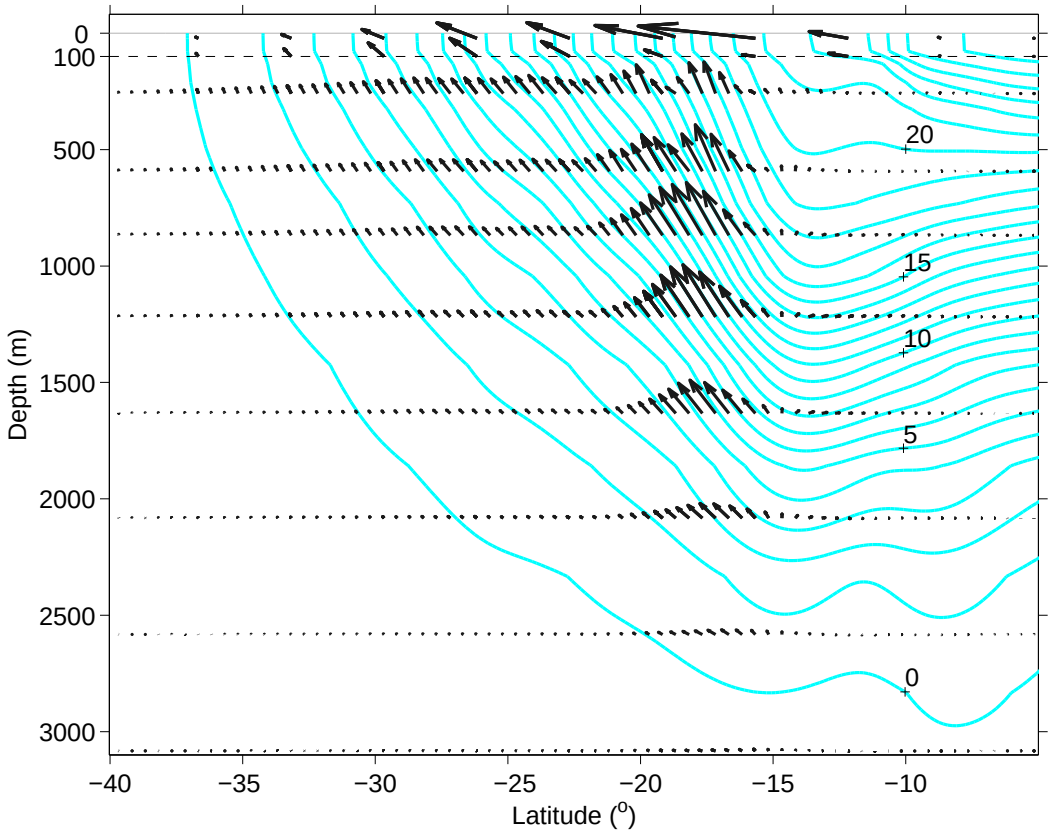

Figure 5: Mean isotherms which coincide with the mean isopycnals (solid line, contour interval 1 ^{o} C) and eddy heat flux $\overline{\mathbf{u}'T'}$ (arrows). In the surface diabatic layer (100 m thick) every other point in depth and every twenty-first latitude point is plotted; in the near adiabatic interior every third latitude point is plotted. The longest arrow corresponds to a heat flux of 0.077 m^o C/s. Light solid line is the surface, dashed line is the base of the surface diabatic layer.

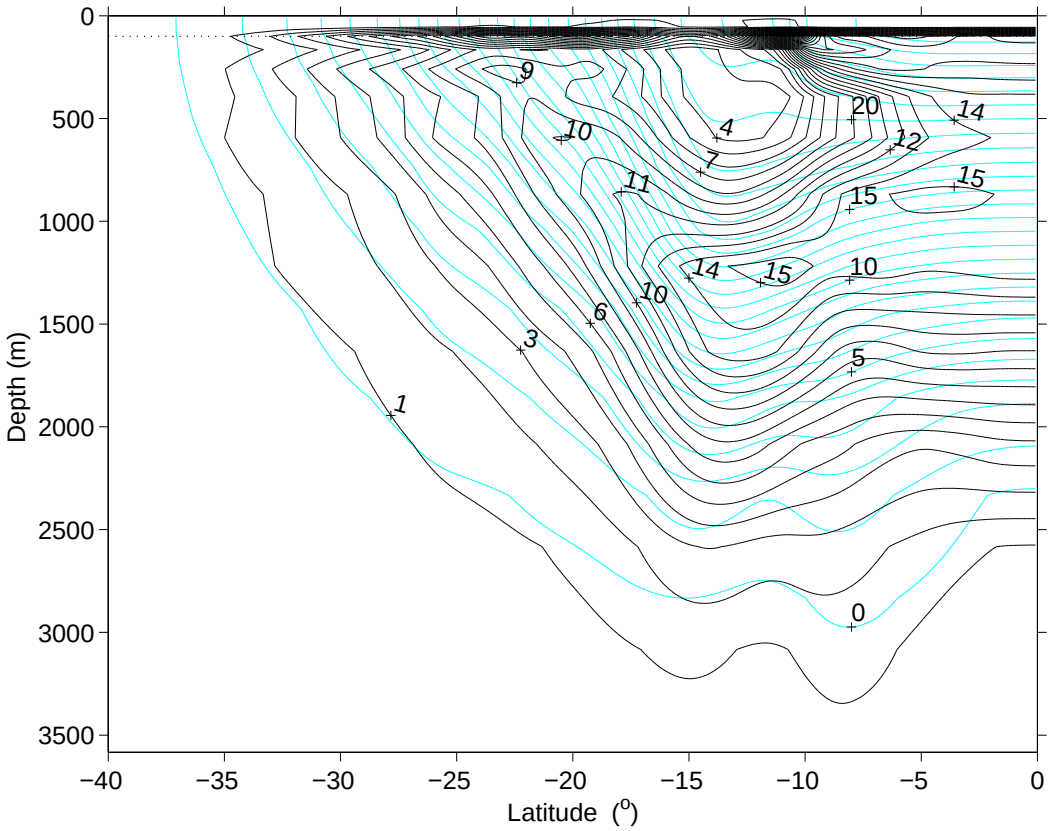

Figure 6: $\partial \bar{T}/\partial z$ (the inverse of mean thickness with the contour interval 10^{-3o}C/m; dark solid line) and mean isopycnals (as in Figure 7, light solid line). Dashed line is the mixed layer base.

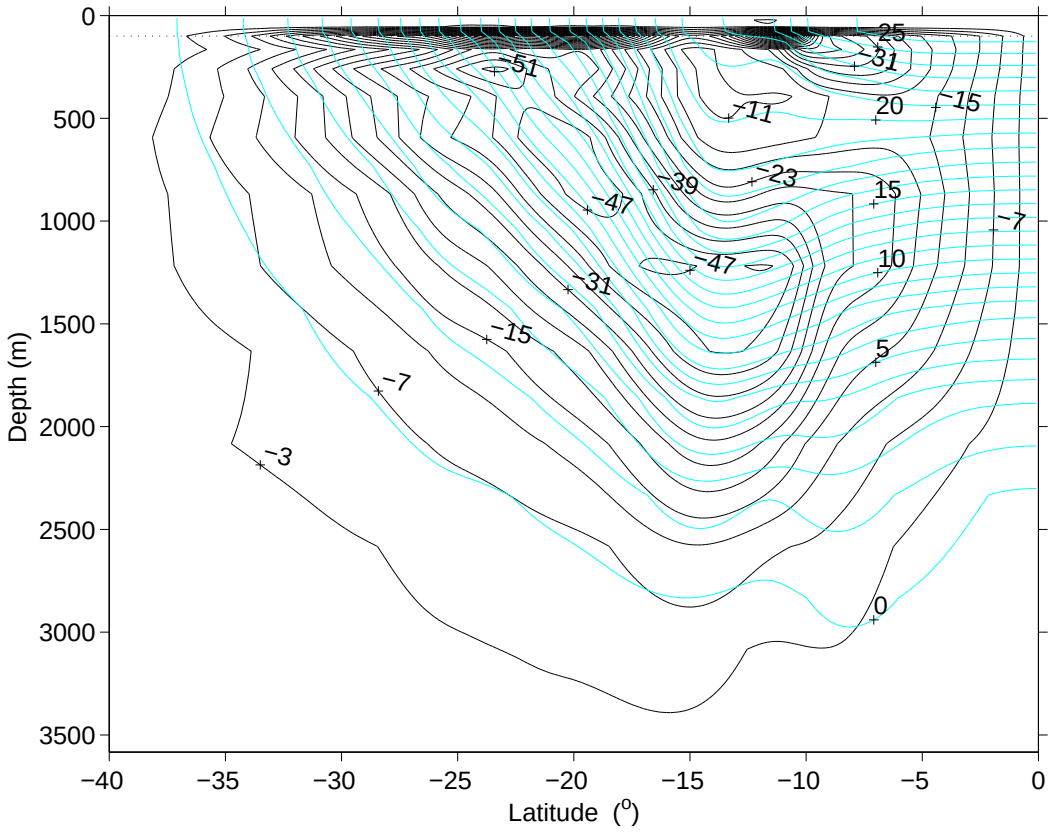

Figure 7: Mean Ertel PV obtained as $\overline{P} = \overline{\zeta_a \cdot \nabla T}$ (dark solid line, contour interval 1.5x10 $^{-8}$ s^{-1} m^{-1} ^{o} C), and mean isopycnals (which coincide with the mean isotherms; in ^{o} C, contour interval 1 ^{o} C, light solid line). Dashed line is the base of the mixed layer at 100 m depth.

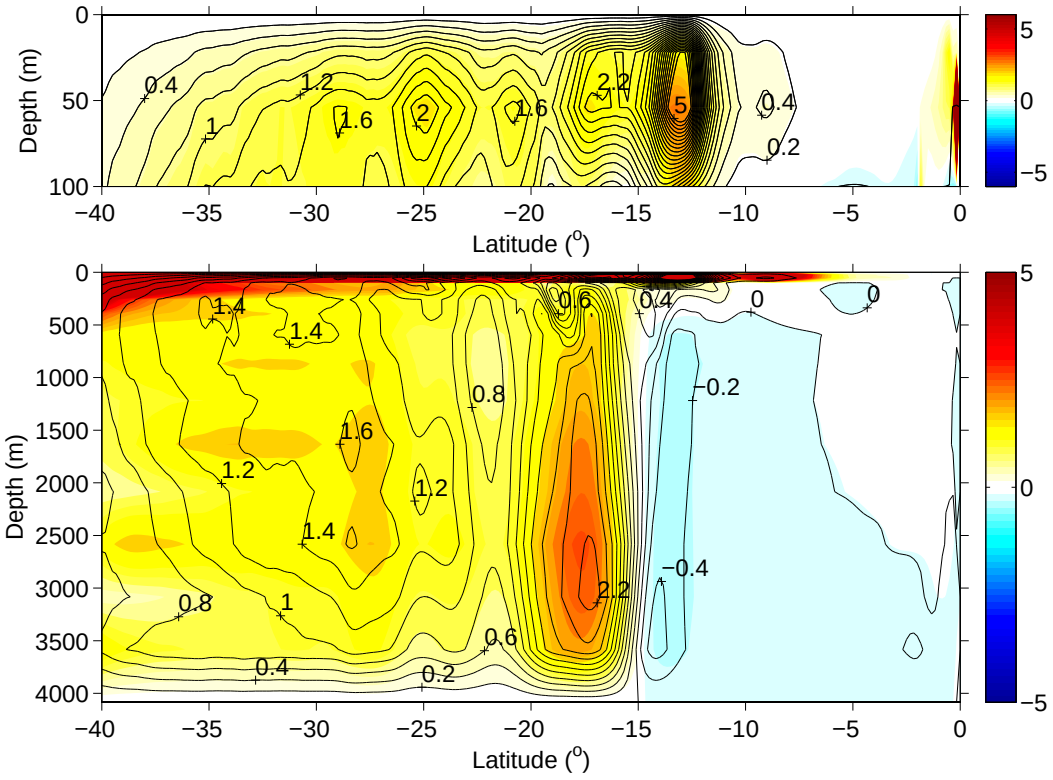

Figure 8: Quasi-Stokes streamfunction defined by (5) plotted as solid contours compared to the Held and Schneider (1999) quasi-Stokes streamfunction plotted in colors in the top panel and quasi-geostrophic streamfunction plotted in colors in the bottom panel. $\gamma = 10^3$in (5). All in $m^2\ s^{-1}$.

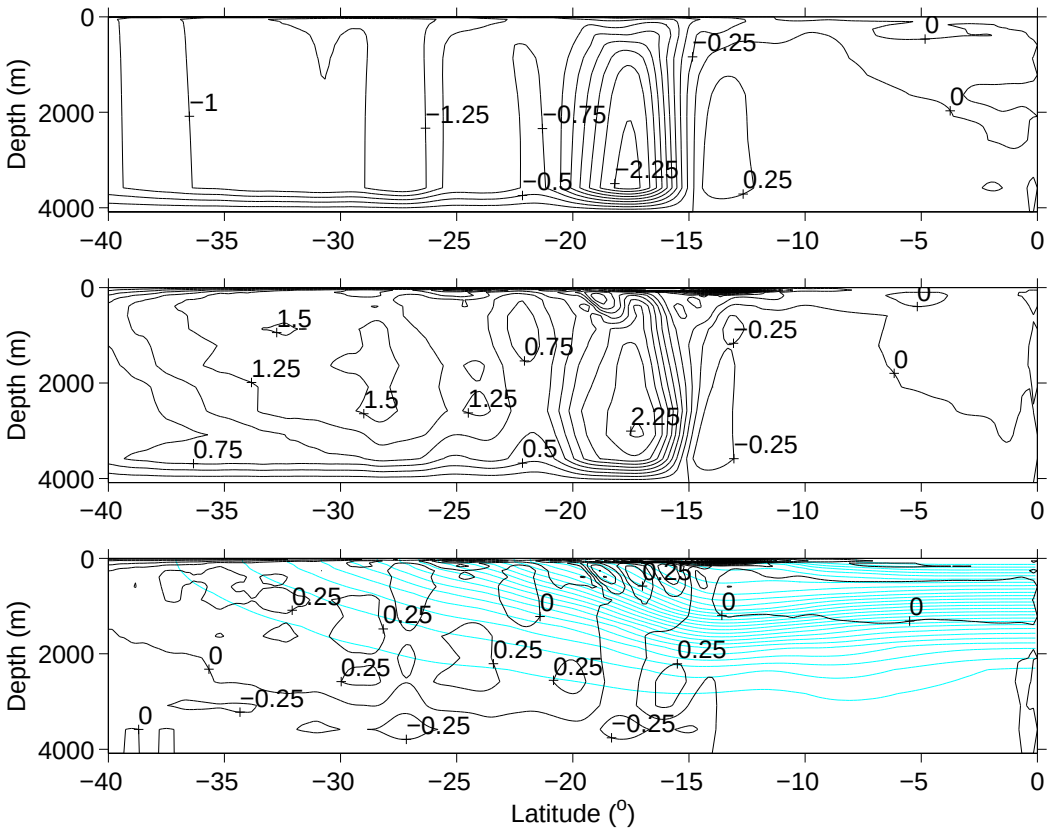

Figure 9: Meridional cross-section of zonally and time averaged velocity streamfunctions: Eulerian (top) and residual streamfunction (bottom). Both in (m^2 s^{-1}). Contour interval is 0.25 m^2 s^{-1}. Velocities are obtained as: $v = \partial\psi/\partial z$, $w = -\partial\psi/\partial y$.

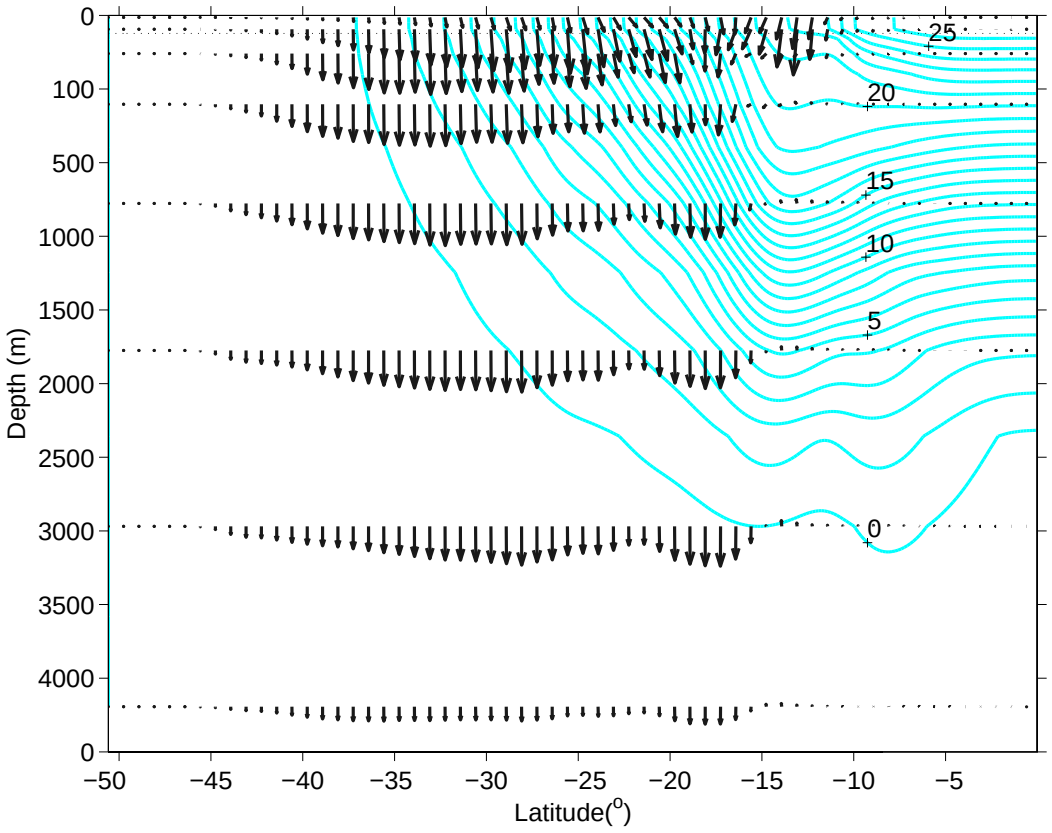

Figure 10: Mean isotherms in ^{o} C (plotted with contour interval 1 ^{o} C) which coincide with the mean isopycnals (solid line) and residual angular momentum flux $\mathbf{F}^{\dagger}\{m\}$ (arrows); the longest arrow corresponds to a flux 1.84x10 ^{4} m^3 s^{-2}. Dotted line is the base of the surface diabatic layer. Residual angular momentum flux is plotted for every other vertical layer starting from layer one and every fifth point in latitude.

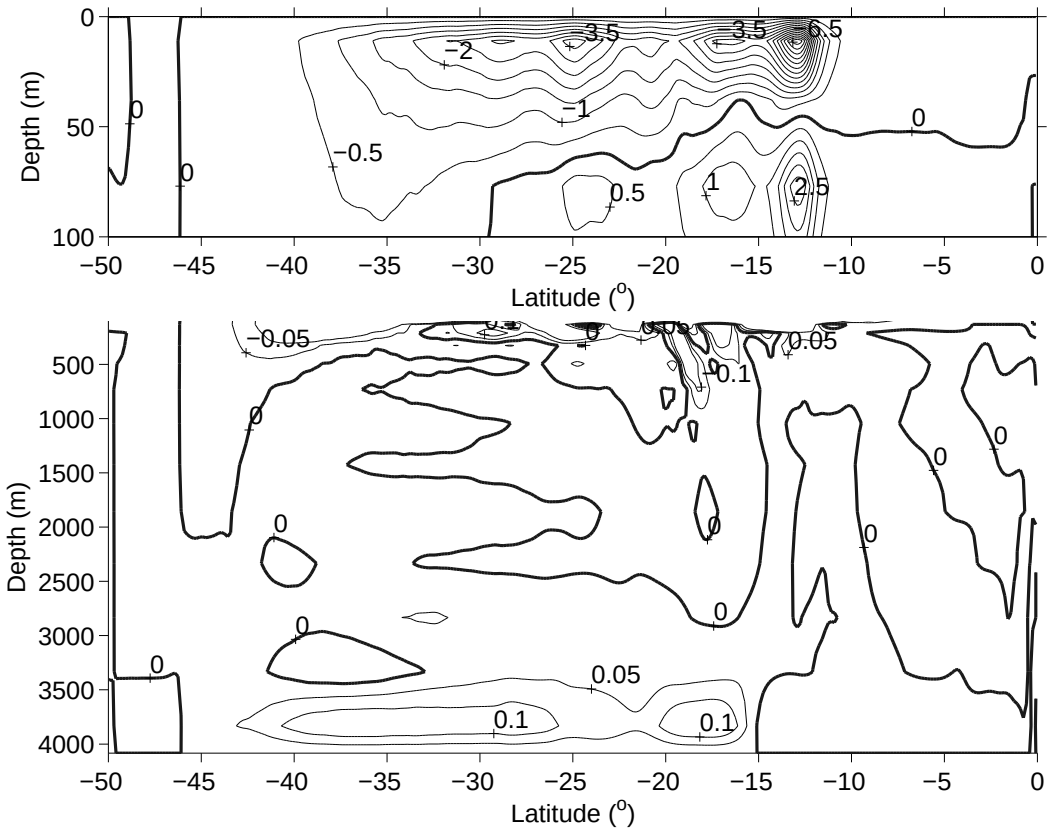

Figure 11: Eddy forcing of mean angular momentum given by $-\nabla \cdot \mathbf{F}^{\dagger}\{m\}$ in the surface diabatic layer (top panel) and in the near-adiabatic interior (bottom panel) in m/s^2. Contour levels are from -6.8 to 2.8 with contour interval of 0.5 m/s^2 (top panel) and from -0.1 to 0.1 with contour interval of 0.05 m/s^2 (bottom panel). Zero contour is plotted as a thick line.

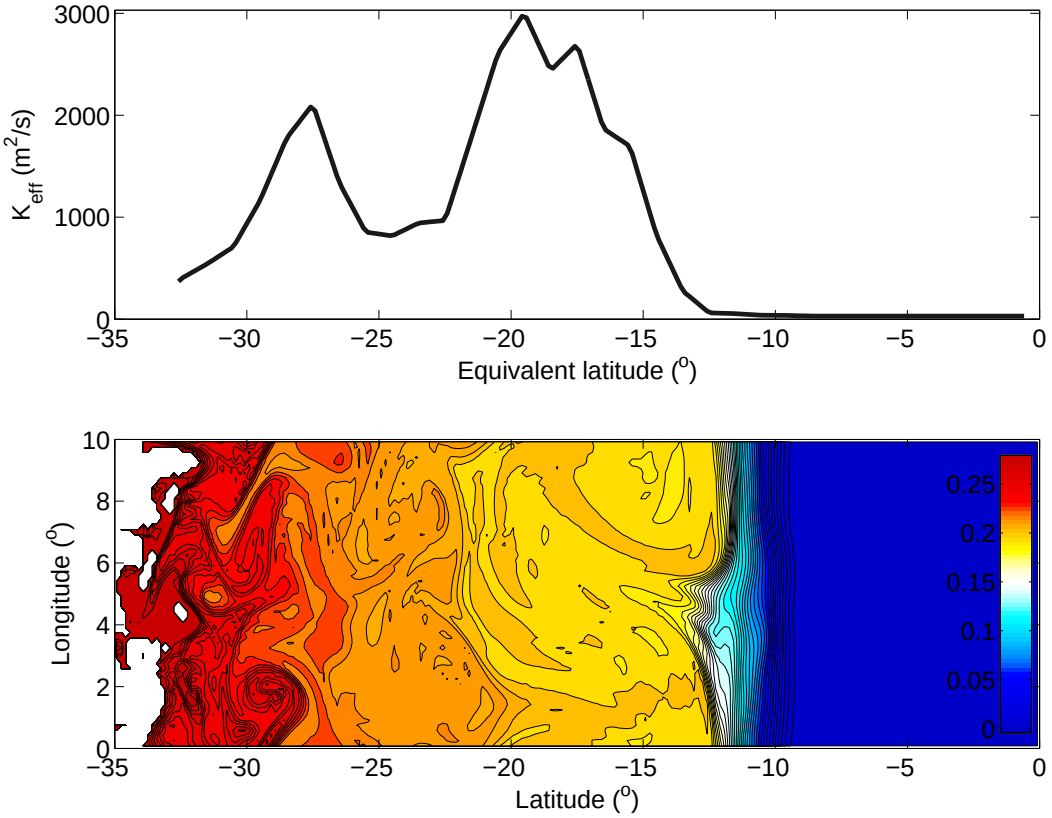

Figure 12: Instantaneous effective diffusivity (in m^2s^{-1}), top panel, obtained by analyzing snap-shot of passive tracer concentrations on 1.3^o C isotherm 70 years after tracer release (bottom panel).

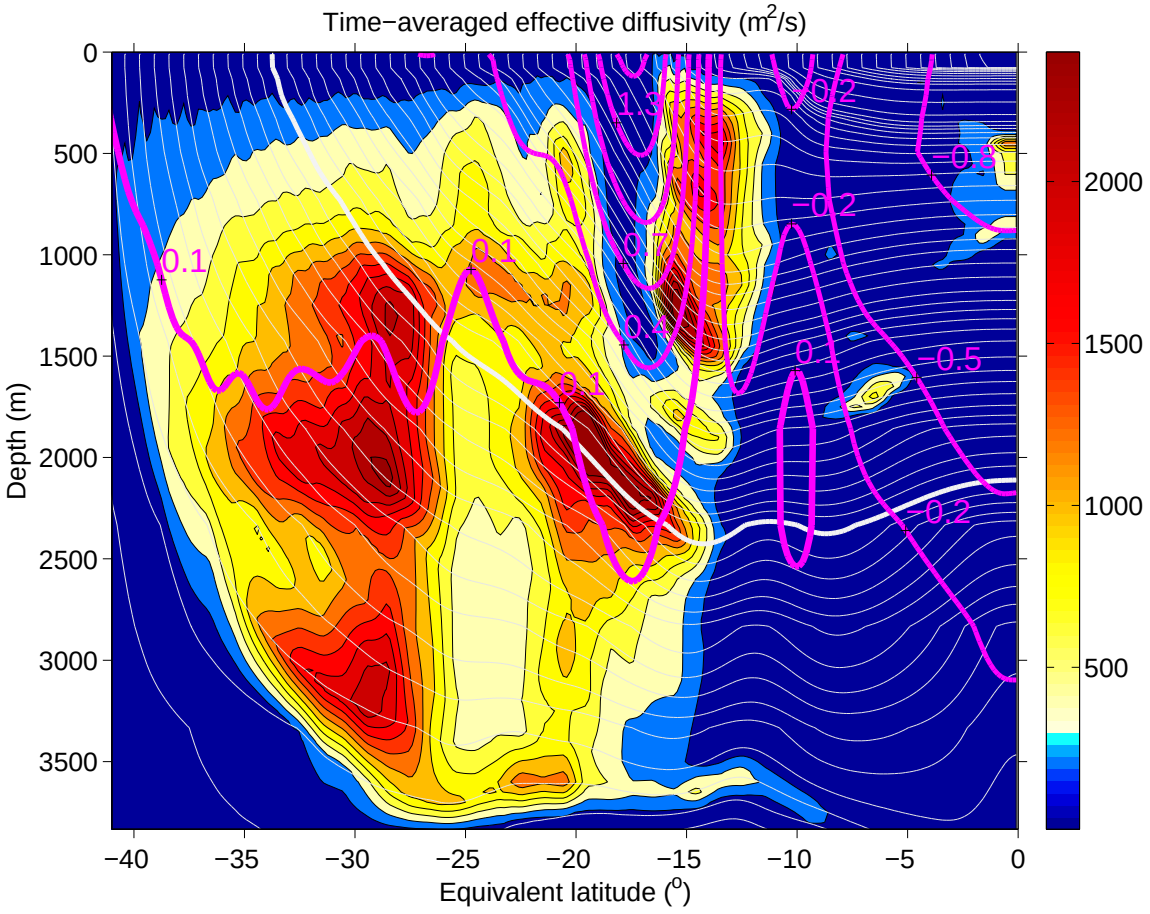

Figure 13: Time-averaged effective diffusivity (in m^2s^{-1}) obtained by analyzing snap-shots of passive tracer concentration taken 1 year apart from 31 to 71 years after tracer release (colours) together with time and zonally averaged zonal velocity (pink line, in ms^{-1}) and time and zonally averaged isotherms on which calculation has been carried out (light gray lines, in ^oC). Thick gray line is 1.3^oC isotherm. Thick yellow line is 0.1 m/s zonal velocity isoline.